





RESEARCH ARTICLE

An in vivo model of ligamentum flavum hypertrophy from early-stage inflammation to fibrosis

Kevin G. Burt^{1,2}  | Dan C. Viola¹  | Lauren E. Lisiewski^{1,2}  |
Joseph M. Lombardi¹ | Louis F. Amorosa³ | Nadeen O. Chahine^{1,2} 

¹Department of Orthopedic Surgery, Columbia University, New York, New York, USA

²Department of Biomedical Engineering, Columbia University, New York, New York, USA

³Ridgewood Orthopaedic Group, Ridgewood, New Jersey, USA

Correspondence

Nadeen O. Chahine, Department of Orthopedic Surgery, Columbia University, 650 West 168th St, 14-1408E, New York, NY 10032, USA.

Email: noc7@columbia.edu

Louis F. Amorosa, Ridgewood Orthopaedic Group, 85S Maple Ave, Ridgewood, NJ 07450, USA.

Email: lamorosa@ridgewoodortho.com

Funding information

National Institutes of Health, Grant/Award Numbers: R01AR069668, R01AR077760, R21AR080516; Orthopaedic Science and Research Foundation (OSRF)

Abstract

Multi-joint disease pathologies in the lumbar spine, including ligamentum flavum (LF) hypertrophy and intervertebral disc (IVD) bulging or herniation contribute to lumbar spinal stenosis (LSS), a highly prevalent condition characterized by symptomatic narrowing of the spinal canal. Clinical hypertrophic LF is characterized by a loss of elastic fibers and increase in collagen fibers, resulting in fibrotic thickening and scar formation. In this study, we created an injury model to test the hypothesis that LF needle scrape injury in the rat will result in hypertrophy of the LF characterized by altered tissue geometry, matrix organization, composition and inflammation. An initial pilot study was conducted to evaluate effect of needle size. Results indicate that LF needle scrape injury using a 22G needle produced upregulation of the pro-inflammatory cytokine *Il6* at 1 week post injury, and increased expression of *Ctgf* and *Tgfb1* at 8 weeks post injury, along with persistent presence of infiltrating macrophages at 1, 3, and 8 weeks post injury. LF integrity was also altered, evidenced by increases in LF tissue thickness and loss of elastic tissue by 8 weeks post injury. Persistent LF injury also produced multi-joint effects in the lumbar IVD, including disc height loss at the injury and adjacent to injury level, with degenerative IVD changes observed in the adjacent level. These results demonstrate that LF scrape injury in the rat produces structural and molecular features of LF hypertrophy and IVD height and histological changes, dependent on level. This model may be useful for testing of therapeutic interventions for treatment of LSS and IVD degeneration associated with LF hypertrophy.

KEYWORDS

fibrosis, histological analysis, hypertrophy, inflammation, ligamentum flavum, rat model

1 | INTRODUCTION

Degenerative lumbar spinal stenosis (LSS) is a common condition in the aging population, estimated to affect almost half of those in the 60–69 year old age group.¹ Narrowing of the spinal canal and the

resulting nerve root compression is responsible for lower back and leg pain and numbness, common symptoms of LSS.² Numerous pathologies contribute to the onset of LSS, such as intervertebral disc (IVD) bulging, facet joint degeneration, and ligamentum flavum (LF) hypertrophy,^{3,4} which broadly alter the spinal geometry and

This is an open access article under the terms of the [Creative Commons Attribution-NonCommercial-NoDerivs](https://creativecommons.org/licenses/by-nc-nd/4.0/) License, which permits use and distribution in any medium, provided the original work is properly cited, the use is non-commercial and no modifications or adaptations are made.

© 2023 The Authors. *JOR Spine* published by Wiley Periodicals LLC on behalf of Orthopaedic Research Society.

encroach on the spinal canal. Of these pathologies, LF hypertrophy is a primary contributing factor to LSS and associated symptoms. This contribution occurs as changes to the LF footprint directly imposes on the natural geometry of the spinal canal, ultimately compressing nerve roots.⁵⁻⁷ In imaging studies, load induced bulging of the LF has been found to contribute 50%–85% of the total narrowing occurring in the spinal canal.⁸ Based on these findings, it was concluded that the LF, not the IVD, is the dominating structure leading to load induced narrowing of the lumbar spinal canal.⁸

The LF is a series of spinal ligaments that connects the laminae of vertebral bodies, bridging the interlaminar space and forming sections of the dorsal border of the spinal canal. In its healthy state, the LF matrix is comprised of 70% elastin fibers and 30% collagen fibers organized in parallel layers, priming the tissue to maintain mechanical stability throughout the spine.^{9,10} Alternatively, in severe diseased patient samples, fibrosis of the entire LF area has been observed, and is characterized by a loss of elastic fibers and increase in collagen fibers.¹¹ Furthering this characterization, fibrotic thickening and scar tissue formation has been identified as the primary pathology of LF hypertrophy,¹² with severity of scarring found to be significantly correlated with LF thickness.¹³ The pathological deposition of extracellular matrix is thought to induce a change in LF geometry, leading to a thickening of the ligament. This is supported by clinical observations in LSS cases which exhibited significant changes in LF transverse area and a near two-fold increase in tissue thickness compared to control LF specimens collected from acute IVD herniation cases.¹⁴ Interestingly, it remains a debate as to whether LF hypertrophy occurs in isolation or as part of multi-joint spinal changes. For example, facet joint changes (e.g., facet hypertrophy) or IVD changes (e.g., disc space narrowing) have both been found to be associated with LF hypertrophy, which is hypothesized to occur by buckling and thickening of the LF.¹⁵ Morphological changes associated with LF hypertrophy can lead to mechanical changes at the spinal level, with potential implications to the integrity of the IVD and facet joint. A reduction in LF stiffness and ultimate strength were found to be correlated with IVD degeneration in human samples.¹⁶ While multi-joint changes consisting of correlations between LF hypertrophy and IVD degeneration have been observed in some studies,¹⁷ other studies do not observe such associations.¹⁸ Moreover, many studies examining LF patient samples *ex vivo* do not address the potential for concomitant change in the IVD. Thus, there remains a gap in knowledge as to whether LF hypertrophy can cause changes in IVD integrity.

While the pathogenesis and related mechanisms of LF hypertrophy are largely unknown, mechanisms involving fibrotic signaling and recruitment of innate immune cells have been implicated. In human hypertrophied LF tissue, inflammatory cell infiltration and increased blood vessel formation is observed, and not evident in healthy human LF control samples.¹⁹ In patient samples, levels of molecular mediators associated with LF fibrosis such as transforming growth factor beta 1 (*TGFB1*), connective tissue growth factor (*CTGF*) and platelet derived growth factor alpha (*PDGFA*), are increased in LF hypertrophy samples compared to controls.²⁰⁻²² Moreover, evaluation of human fibrotic LF tissue revealed increased expression of pro-inflammatory cytokine

genes including cyclooxygenase-2 (*Cox2*), tumor necrosis factor- α (*Tnfa*), and interleukin-6 (*Il6*).¹³ Though analysis of human LF patient samples provides insight to the disease state, the inability to study longitudinal changes in patient samples limits the scientific understanding of LF hypertrophy etiology. Further, 2D & 3D cultures provide potential for investigating responses of human LF cells to inflammatory soluble factors or induced mechanical loading at the cellular level,^{23,24} however *in vitro* studies do not fully recapitulate the pathological *in vivo* tissue microenvironment, presenting a clear need for animal models of LF hypertrophy.

Mechanical overuse has been used as a clinically relevant stimulus to induce LF injury and hypertrophy in rodent models. Applied flexion-extension overuse of the mouse lumbar spine was found to increase LF thickness and collagen fiber area.²⁵ However, in this mechanical stress model, there was no evidence of macrophage infiltration, angiogenesis, or increase in the expression of transforming growth factor beta 1 (*Tgfb1*), which are characteristic features of LF hypertrophy in patient samples.²⁵ Subsequent studies in the mouse using needle micro-injury methods resulted in LF hypertrophy that was dependent on early macrophage infiltration.^{25,26} However, limitations in the mouse exist due to anatomical differences between human and mouse LF footprint within the spinal canal.²⁵ Alternatively, larger rodent models, such as the rat, more closely represent the human LF in terms of histological features, anatomical position, and tissue composition, and may be more useful for evaluating therapeutic interventions.^{27,28} In the rat, Sato *et al* found that posterior destabilization of lumbar spine intended to increase flexion and thus cause overloading on the LF, caused enlargement of the dorsal surface layer of the LF. However, changes to the mid-substance of the LF ECM was not investigated. Recent studies by Wang *et al*, tested the effect of increased lumbar segment motion by resection of spinous process, grinding of facet joints and removal of paraspinal muscle.²⁷⁻²⁹ This approach resulted in LF hypertrophy, with increased LF thickness and area, increased area of matrix containing collagen fibers, but no change in area containing elastic fibers, suggesting that this model simulated mild LF hypertrophic changes. Interestingly, this model also increased gene expression of pro-inflammatory cytokines (*Tnfa*, interleukin 1 beta: *Il1b*) and factors promoting fibrosis (*Tgfb1*), however, longitudinal changes over time were not investigated. While the study demonstrated increased motion with higher disc height ratio in the experimental group compared to sham, the effects of increased motion on IVD integrity was also not investigated.

The goal of this study is to investigate the effect of needle scrape injury to rat lumbar LF on longitudinal changes in LF morphology, ECM deposition, fibrosis and pro-inflammatory expression, and simulating LF hypertrophy. It was hypothesized that structural disruption of the LF via needle scrape will produce an observable early inflammatory response and later stage tissue fibrosis, that simulate changes observed in patient samples of LF hypertrophy. Initially, we evaluated the response of LF to needle gauge size. We next performed longitudinal analysis of the progression in injury response up to 8 weeks. Lastly, we investigated concomitant changes in IVD integrity in the LF injury model.

2 | MATERIALS AND METHODS

2.1 | Pilot injury study

Institutional Animal Care and Use Committee approval was obtained for all animal work prior to start of the study. Eighteen male Sprague Dawley rats (3–4 months of age) were used during an initial pilot study. Animals were housed in a temperature and humidity-controlled environment subject to 12 h light/ 12 h dark cycles. Prior to surgical procedures, an analgesic (Buprenorphine SR, 1.0 mg/kg) was administered via intraperitoneal injection. During surgical procedures, animals were subjected to inhalant anesthesia (Isoflurane, 2%–5%). A 2 cm surgical incision in the midline was made over the spinous processes of L3 and L4, and confirmed with lateral fluoroscopy (OEC Medical Systems, MiniView 6800). While utilizing a surgical microscope (Zeiss Model S5), muscles were subperiosteally dissected off the spinous process and the lamina to expose the interlaminar space, while preserving the midline interspinous and supraspinous ligaments. Animals were randomized into either (1) 22G injury, (2) 30G injury, or (3) sham group. Within injury groups, four passes were made with a 22G or 30G needle along the LF in the caudal to cranial direction, creating a scrape injury. Within the control (sham surgery) group, animals received analgesic, were anesthetized, and underwent a 2 cm surgical incision with midline exposure before wound closure (no needle scrape). Animals within the pilot study were returned to cage activity for 1 week prior to euthanasia ($N = 6$ per group). To help ascertain a potential effect of the sham surgery on histological outcomes, the lumbar spine from age- and weight- matched rats that did not undergo surgery (negative control, $N = 2$) was also collected for histological comparison.

2.2 | Longitudinal injury study

Twenty-four male Sprague Dawley rats (3–4 months of age) were used for the longitudinal LF injury study. Animal housing and surgery approval was obtained as described in the pilot study. Injury using the 22G needle and sham groups were performed as described above. Following surgery, 22G injury and sham groups euthanized, via CO₂ inhalation, at 3 or 8 weeks post injury ($N = 6$ per group and time point).

2.3 | Disc height analysis

All animals underwent lateral fluoroscopic imaging of the lumbar spine for radiographic measurements prior to surgery and at time of euthanasia ($N = 6$ per group and time point). A disc height index (DHI) was obtained from images in the sagittal plane, by averaging measurements from anterior, middle and posterior portions of the IVD and dividing the measurements by the average of adjacent vertebral body heights.³⁰ To achieve repeatable images in the lateral view animals were positioned in lateral decubitus while keeping the physiological

lumbar spine in flexion. The iliac crest alignment and lumbar spinous processes were used as anatomical landmarks to confirm lateral decubitus. The x-ray was centered on the iliac crest and images were evaluated to ensure (1) iliac crest overlap, (2) spinous process with no rotation, and (3) the lateral process of lumbar vertebrae having an ovoid shape. A ratio of post-surgery to presurgery DHI was calculated at the injury level (L3-L4) and at immediate superior (L2-L3) and inferior levels (L4-L5). Changes to DHI ratio allowed for evaluation of disc height changes due to sham procedure or LF injury at 1, 3, and 8 weeks.

2.4 | LF histomorphology analysis

The L2-L5 spine segment containing the injured and immediate superior and inferior adjacent levels, were dissected out. Spine segments ($N = 3$ per group and time point) were then fixed in 4% paraformaldehyde (PFA) for 48 h, decalcified in 14% ethylenediaminetetraacetic acid (EDTA) for 1–2 weeks, and paraffin embedded. Lumbar spine segments were then sectioned and stained for histological analyses with H&E, Mason's Trichrome or elastin van Gieson (EVG), as described below. Images were acquired with a digital imaging microscope (Leica SCN400) capturing multiple bright field images at 40 \times (0.25 $\mu\text{m}/\text{pixel}$) and stitched together to produce whole slide images. LF geometric analysis was performed on H&E-stained sagittal histological sections taken through the midline using ImageJ software. LF thickness was calculated as the average of three measurements taken from the edge of the spinal canal in the dorsal direction towards the opposite LF edge and interspinous ligament. Cross-sectional area was measured as the region of interest outlining the LF footprint. H&E-stained sections were also used for a grading of LF morphology, structure, and degree of elastic fiber degradation, with higher scores indicating more elastic fiber degradation (Figure S1).³¹ All histological evaluations were done by a blinded trained researcher with expertise in histological analysis of IVD and ligament tissue morphology.

2.5 | Fibrotic LF tissue analysis

Masson's Trichrome (MT: keratin, muscle, and collagen) staining was utilized for analysis of the degree of fibrosis (range 0–4) evaluating elastic fiber and collagen staining intensity throughout the LF, with higher scores representing increased fibrosis (Figure S1) ($N = 3$ per group and time point). MT stains were evaluated for fibrotic tissue regions with “no fibrosis” assigned a grade of “0,” fibrosis in 25% the observed area assigned a grade of “1,” 25%–50% assigned a grade of “2,” 50%–75% assigned a grade of “3,” and >75% fibrosis observed in tissue region assigned a grade of “4.”¹³ EVG (elastin) staining was utilized for an elastin grading (range 0–4), assessing elastic tissue fiber alignment, fragmentation, and abundance throughout the LF (Figure S1). Higher elastin grading scores represented increased tissue hypertrophy and elastic tissue degradation, where a grade of “0” represented samples completely positive for elastin (black) with

increasing grades being associated with gradual elastin loss. A grade of “4” represented samples with minimal elastin staining.¹³

2.6 | LF gene expression

Whole LF tissue segments were dissected from the injury level or equivalent level in sham animals ($N = 3$ per group and time point) immediately after euthanasia and were snap-frozen and stored at -80°C for later RNA isolation. LF tissue was pulverized using a bead tissue homogenizer (Mikro-Dismembrator U, Sartorius). Total RNA was isolated using TRIzol (ThermoFisher) and chloroform phase separation with RNA cleanup via spin columns (Qiagen) per manufacturer's instructions. RT-QPCR was performed as follows, complementary DNA reverse transcription using Iscript cDNA synthesis kit (Bio-rad) and real time PCR via Iqaa Universal SYBR kit (Bio-rad) per manufacturer's instructions. Rat specific primers for hypertrophic markers, collagen type I alpha 1 (*Col1a1*, FWD: GCT TGA AGA CCT ATG TGG GTA TAA, REV: GGG TGG AGA AAG GAA CAG AAA), collagen type III alpha 1 (*Col3a1*, FWD: CAG GCC AAT GGC AAT GTA AAG, REV: GCC ATC CTC TAG AAC TGT GTA AG), connective tissue growth factor (*Ctgf*, FWD: AGG GAC ACG AAC TCA TTT AGA C, REV: CAG CAG TTA GGA ACC CAG ATT), platelet derived growth factor alpha (*Pdgfa*, FWD: CCA GCG ACT CTT GGA GAT AGA, REV: TTC TCC GGC ACA TGC TTA AC), transforming growth factor beta 1 (*Tgfb1*, FWD: CTG AAC CAA GGA GAC GGA ATA C, REV: GTT TGG GAC TGA TCC CAT TGA), actin alpha 2 (*Acta2*, FWD: CCT CTT CCA GCC ATC TTT CAT, REV: CGA GAG GAC GTT GTT AGC ATA G) and inflammatory markers, tumor necrosis factor alpha (*Tnfa*, FWD: CCC AAT CTG TGT CCT TCT AAC T, REV: CAG CGT CTC GTG TGT TTC T), interleukin-1 beta (*Il1b*, FWD: TCT GAC AGG CAA CCA CTT AC, REV: CAT CCC ATA CAC ACG GAC AA), and interleukin-6 (*Il6*, FWD: GAA GTT AGA GTC ACA GAA GGA GTG, REV: GTT TGC CGA GTA GAC CTC ATA G) were used. Gene expression values were normalized to glyceraldehyde-3-phosphate dehydrogenase (*Gapdh*, FWD: GCA AGG ATA CTG AGA GCA AGA G, REV: GGA TGG AAT TGT GAG GGA GAT G) relative to sham controls.

2.7 | Immunofluorescence microscopy

Paraffin embedded tissue sections were baked at 60°C for 30 min, deparaffinized with xylene, and rehydrated using graded series of ethanol washes. Antigen retrieval was performed with hyaluronidase at 37°C for 12 min followed by 0.1% Triton-X at room temperature for 5 min. Tissue sections were blocked for nonspecific binding using background buster (Innovex Biosciences) at room temperature for 45 min. Sections were then incubated overnight at 4°C with primary antibodies for the general leukocyte marker, CD45 (Abcam, AB10558, 1:100) or the pan-monocyte/macrophage marker, CD68 (Abcam, AB955, 1:100). The next day, sections were incubated for 1 h at room temperature with secondary fluorescent antibodies goat anti-rabbit Alexa Fluor (AF) 488 (Abcam, AB150081, 1:100) or goat anti-mouse AF595 (Invitrogen, A-11005, 1:100). Sections were mounted with

VECTASHEILD DAPI anti-fade mounting medium (Vector, H-1200) and allowed to set for 30 min before imaging with an Axio Observer (Zeiss) using $20\times/0.5$ Plan-Neofluar or $10\times/0.25$ A-Plan objectives (Axiocam 702 mono camera), and Zen software. Exposure settings were fixed across all tissue sections during imaging.

2.8 | Intervertebral disc histological scoring

Histological grading of IVDs was performed at the injury level (L3-L4) and at immediate proximal (L2-L3) and distal levels (L4-L5) ($N = 3$ per group, level and time point). Histological grading evaluated changes in cellularity and morphology of the AF, integrity of border between AF and nucleus pulposus (NP), and cellularity and morphology of the NP, with higher scores representing increased degeneration.³⁰ Grading ranged from 5 to 15, where a healthy grade was assigned to IVDs with an AF comprising primarily of elongated fibroblast-like cells, well-organized collagen AF lamellae, an uninterrupted AF-NP border, highly cellular and evenly distributed NP comprising of at least half the IVD area in midsagittal sections. Degenerated IVDs exhibited an AF containing primarily chondrocyte-like cells, inward bulging and disorganized AF lamella structure, interrupted AF-NP border, loss of NP cellularity with increased cell clustering, and an irregularly NP shape comprising of less than 25% of IVD area in midsagittal sections.

2.9 | Statistics

Differences between groups were analyzed with Student's *t*-test with $p < 0.05$ considered significant. To assess (a) differences across time points and group or (b) differences between spinal levels and group, a two-way ANOVA was used with Fisher's LSD post hoc analysis with $p < 0.05$ considered significant. To assess potential relationships within LF related outcomes and their relationship to the IVD, study outcomes were analyzed using Spearman correlation tests. Spearman *r* correlation values (r_s) between measured variables were interpreted to be small ($0.1 < r_s < 0.29$), medium ($0.3 < r_s < 0.49$) or large ($r_s \geq 0.5$) effect size correlations between the measured variables.³² Significance was defined as correlations with $p < 0.05$. Statistical analyses were performed using GraphPad Prism (V8.3.1).

3 | RESULTS

3.1 | Pilot study—Effect of needle size on early LF injury

Initial analysis evaluating LF injury performed using 22G and 30G needles revealed an observable disruption of the LF footprint in both lesion groups when compared to sham (Figure 1A–C). In geometric analysis, 22G needle significantly increased LF thickness following injury, when compared to sham ($p = 0.020$, Figure 1G). However, the LF thickness of the 33G injured group was comparable to sham group

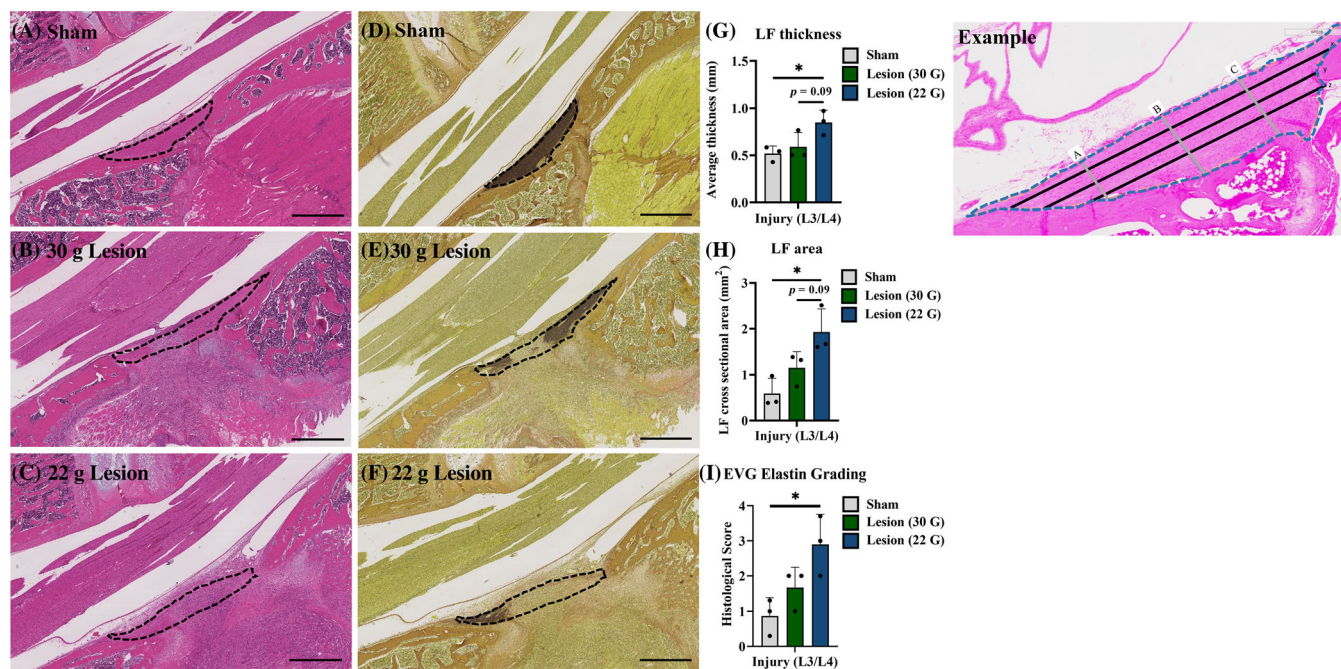


FIGURE 1 Representative LF geometric analysis and calculation (Example): Cross-sectional area was measured within the dashed blue line using ImageJ software analysis. LF thickness was calculated as the average taken across three measurements (labeled in Example as A, B, C). In geometric analysis the 22G lesion group increased LF thickness (G) and cross sectional area (H) compared to sham (A). The 22G injury group produced the greatest disruption of elastin presence and alignment when compared to 30G lesion and sham groups (D–F). The 22G lesion group caused an increase in EVG elastin grading scores when compared to sham (I). Scale bar = 1 mm. * $p < 0.05$, Student's *t*-test.

($p = 0.51$). Similarly, the LF cross-sectional area in 22G group significantly increased compared to sham ($p = 0.019$, Figure 1H), with no significant differences observed between the 30G and sham injury groups (Figure 1H). There were no significant differences in LF thickness or cross-sectional area when comparing 22G and 30G injury groups (Figure 1G,H). In further histological analysis of elastin fiber orientation, both 22G and 30G lesion groups had an altered pattern and orientation of elastin fibers (Figure 1D–F). The increased severity and footprint of needle injury in the 22G needle led to an increase in EVG elastin grading, while no changes were observed in the 30G group compared to sham (Figure 1I). The EVG staining pattern in sham group was also comparable to the LF from negative control group (Figure S3).

3.2 | Longitudinal analysis of needle injury

A longitudinal analysis of LF responses to 22G injury was performed at 3 and 8 weeks post injury compared to sham. 22G injury produced a disruption of LF tissue morphology, including changes in fiber alignment and cellularity in lesion groups compared to sham (Figure 2A–D). In addition to the increase in LF thickness at 1wk, 22G lesion increased LF thickness at 8 weeks ($p = 0.0052$) but not 3 weeks time point (Figure 2E). Regionally, significant increase in LF thickness was observed at 3 weeks post injury in the adjacent lower level, distal to the level of injury (Figure 2E). While LF cross sectional area was significantly increased at the 1wk post injury, further

changes were not evident at later time points. Moreover, no changes between lesion and sham groups were observed in the cross-sectional area at the adjacent levels (Figure 2F).

LF tissue morphology and elastic tissue presence was assessed in H&E-stained sections. In the H&E analysis, the appearance of LF tissue in sham group was similar to that from uninjured animals (negative control, Figure S3). The 22G injury group exhibited unaligned and disrupted LF fiber alignment at 1, 3, and 8 weeks, and a decrease in elastic fiber (pink) stain intensity (white arrows) at 3 and 8 weeks (Figure 2A–D). An infiltrating cell population, indicated by the nuclear counter stain, was most notably observed in the 22G injury group 1 week following injury (Figure 2B). Quantifying changes using histological grading showed that the 22G injury group produced more degraded histological scores at 1 ($p = 0.026$), 3 ($p = 0.047$), and 8 weeks ($p = 0.013$), when compared to sham (Figure 2G). No changes in LF morphology and associated histological scoring were observed between the injury and sham groups in adjacent LF levels (Figure 2G). No major differences in LF morphology was observed at levels adjacent to injury at 8 weeks when compared to sham (Figure S2).

Histological staining specific for collagen and elastin fiber content in MT-stained sections was used to quantify the degree of fibrosis following injury. A healthy LF was observed in the sham groups with low levels of collagen (blue) and high levels of elastic fiber (pink) staining (Figure 3A). At 1 week, a marked increase in cellularity (nuclear counter stain: red), and slight changes to elastic fiber and collagen staining were observed within the lesion group compared to sham (Figure 3B). At 3 and 8 weeks time points,

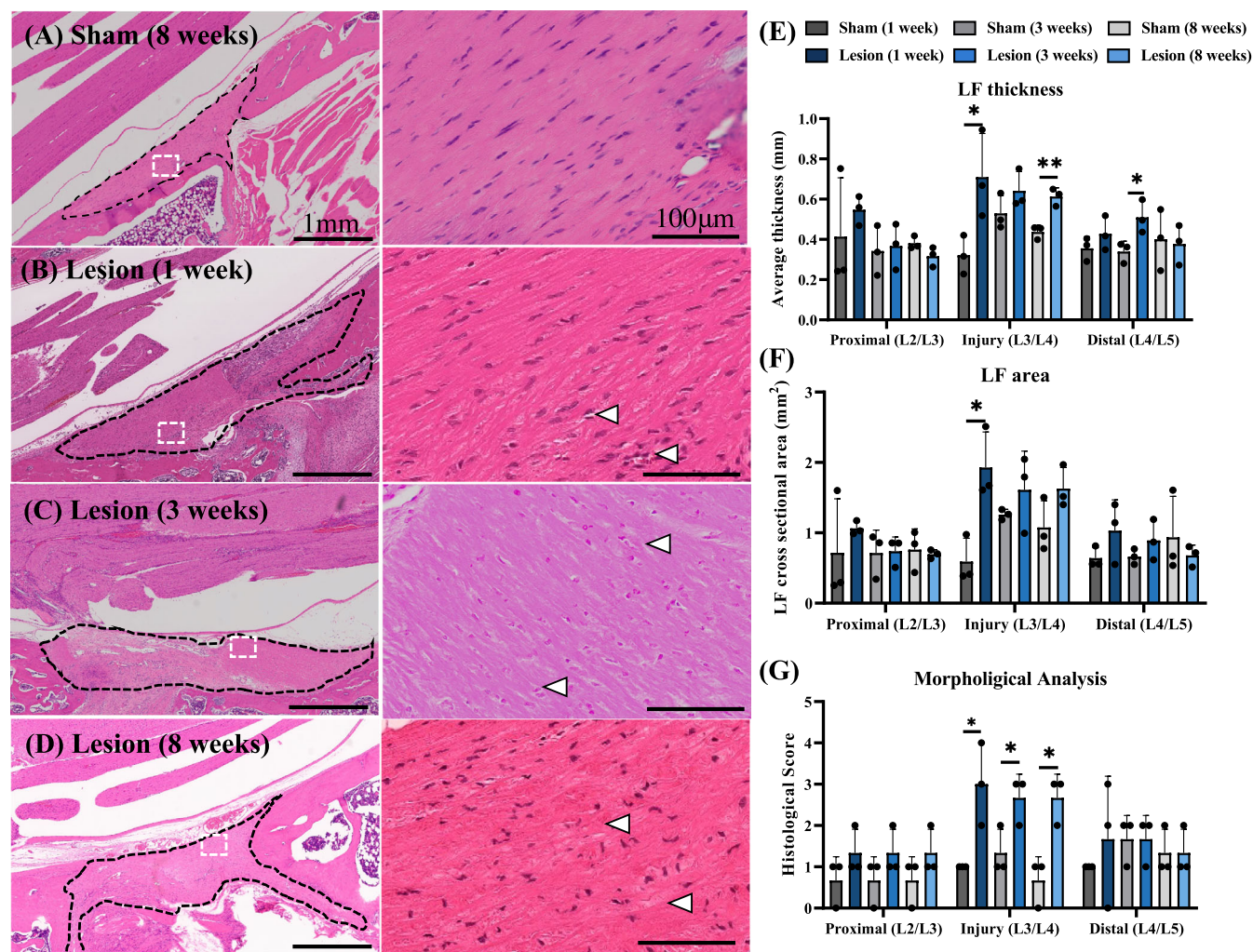


FIGURE 2 Histological scoring of LF structure and morphology using H&E stained sections. Morphological analysis of the LF following lesion revealed a disruption of LF fiber alignment and loss of elastic tissue staining (white arrows) at 1 (B), 3 (C), and 8 weeks (D) when compared to sham (A). In geometric analysis, lesion increased LF thickness at 1 and 8 weeks time points at the injury level, and at 3 weeks in the distal to injury level (E). Lesion increased LF area at 1 week when compared to sham, with no changes observed in the adjacent levels (F). At the injury level 1, 3, and 8 weeks lesion groups had higher histological scores when compared to sham within each time point (G). No changes in histological scoring was observed in the adjacent LFs segments within lesion groups compared to sham. * $p < 0.05$ ** $p < 0.01$, Student's t -test. Scale bars as indicated in (A).

increases in collagen staining, and decreases in elastic fiber staining intensity were observed (Figure 3C,D). In quantifying fibrotic scores, no significant difference was observed between sham and lesion groups across time points (Figure 3E). Further, no changes between sham and lesion groups were observed in the adjacent LF levels evaluated (Figure 3E, S2).

An evaluation of elastin morphology in EVG stained sections revealed healthy aligned elastin fiber (brown-black) morphology throughout the LF in the sham groups (Figure 4A), which was similar to the morphology of LF in uninjured lumbar spines (negative control, Figure S3). However, disruption of the LF was evident in the lesion groups at 1, 3, and 8 weeks time points (Figure 4B–D). Disruption of elastic fibers within the injury site was indicated by presence of short, fragmented fiber length, unaligned fiber orientation, and an overall decrease in elastin fiber presence (intensity) at the injury site (Figure 4B–D). This disruption of LF morphology led to significantly

higher, more degenerated, histological scoring in the 1 week ($p = 0.025$), 3 weeks ($p = 0.0075$), and 8 weeks ($p = 0.0013$) lesion groups compared to their respective sham groups (Figure 4E). Again, no significant changes in elastin fiber disruption was observed in the adjacent LF levels of the injured groups at any time point, when compared to sham (Figure 4E, S2).

3.3 | Gene expression analysis

Gene expression analysis within the injured and sham LF at the injury level demonstrated changes in both inflammatory and fibrosis genes at various time points. Needle lesion increased hypertrophic markers, *Ctgf* ($p = 0.008$) and *Tgfb1* ($p = 0.036$), at 8 weeks following injury (Figure 5A). Evaluating inflammatory gene expression following injury, lesion increased *Il6* ($p = 0.030$) expression at 1 week

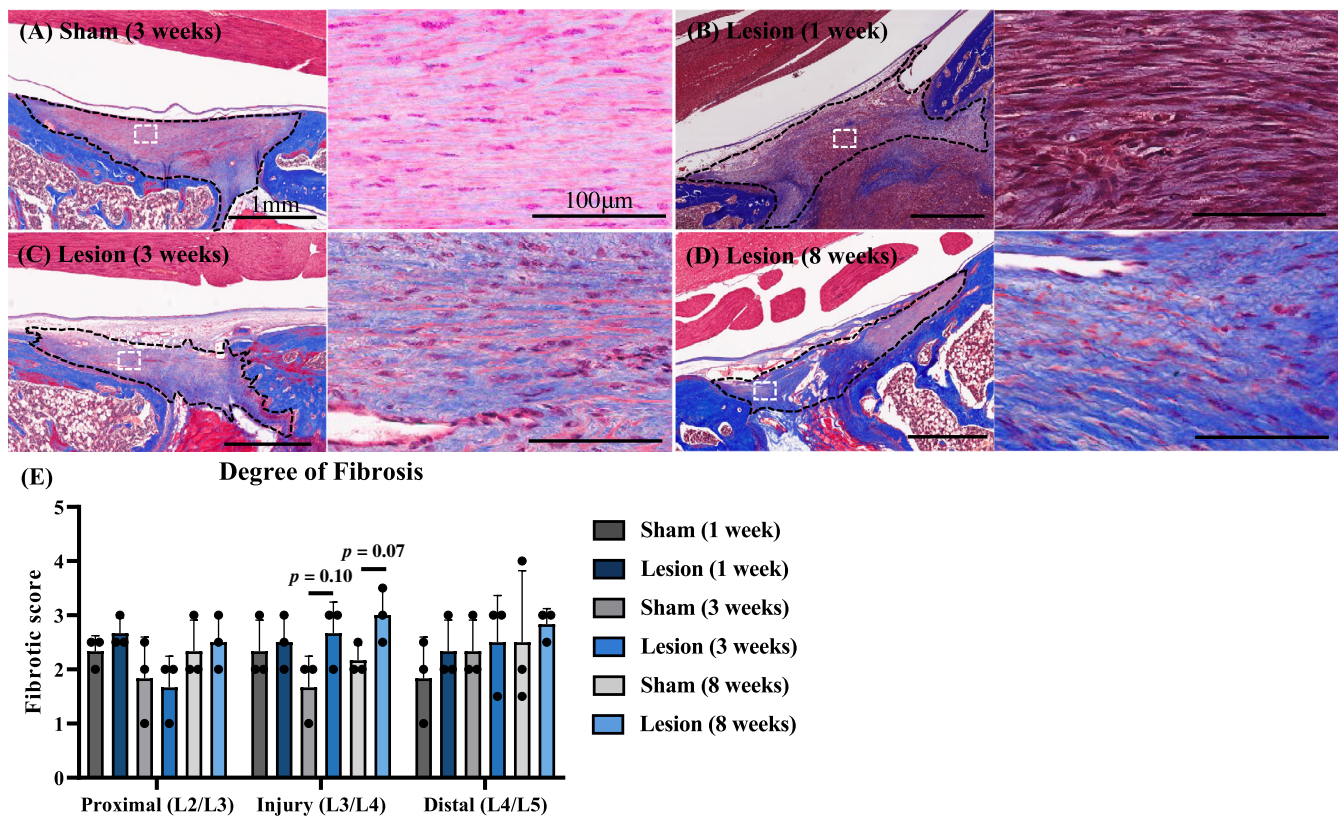


FIGURE 3 Degree of fibrosis evaluation. Histological scoring of hypertrophy using MT stained histological sections of the LF at midline. Lesion produced a noticeable increase in cellularity within the LF as observed through increased nuclear stain when compared to sham (A, B). Lesion produced a loss of elastic tissue (pink) staining intensity and an increase in collagen (blue) staining intensity at 3 and 8 weeks when compared to sham (A, C, D). No statistical significance was observed between groups. A p -value as indicated, Student's t -test. Scale bars as indicated in (A).

following injury, which was not observed following 3 and 8 weeks. Expression of other inflammatory targets (*Tnfa* and *Il1b*) was unchanged (Figure 5A).

3.4 | Inflammatory cell presence

To identify whether the observation of increased cellularity was associated with immune cell infiltration, immunostaining for the common leukocyte antigen, CD45, and pan-macrophage marker, CD68, was performed. Results show the presence of cells positive for both CD45⁺ and CD68⁺ within the injured LF samples, at 1, 3, and 8 weeks following injury (Figure 5B, white arrows). Analysis of sham group samples at all time points did not yield evidence of cells positive for CD45 or CD68. Sections from both groups exhibited nonspecific fluorescence outside the LF region, potentially indicative of bone marrow or red blood cell autofluorescence.

3.5 | Regional IVD integrity following LF injury

Changes to IVD integrity was first assessed by changes to disc height measured via fluoroscopy x-ray images. At the injury level, both sham

and lesion surgeries produced significant decreases across time within groups, with a decrease in DHI ratio between 1 and 3 weeks ($p = 0.042$) and 1 and 8 weeks ($p = 0.014$) in the sham group, and between 1 and 8 weeks in the lesion group ($p = 0.014$) (Figure 6G). Further, in comparing across groups at the injury level, lesion surgery produced a decrease in DHI ratio at 1 ($p = 0.033$), 3 ($p = 0.04$), and 8 weeks ($p = 0.034$) in lesion compared to sham (Figure 6G). In the distal to injury adjacent level (L4/5), lesion surgery produced a significant decrease in DHI ratio over time, when comparing 1 and 3 weeks ($p = 0.042$) and 1 and 8 weeks ($p = 0.025$) lesion groups. A significant decrease in DHI ratio was also observed when comparing sham versus lesion groups at 8 weeks ($p = 0.017$) at the level distal to injury (Figure 6G).

Structural IVD integrity was also evaluated via histological analysis of MT-stained histological sections. Analysis of AF cellularity and structure revealed minimal to no changes when comparing sham versus lesion groups across IVD level and time. Mild degeneration changes within the NP were observed in proximal and injury level lesion groups at 8 weeks, including a decrease in cellularity with increased clustering and disruption to the relatively even cell distribution (Figure 7B,C). This led to a significant increase in histological scoring when comparing proximal lesion to proximal sham groups at 8 weeks ($p = 0.0067$) (Figure 7E). No significance was observed across any other comparisons.

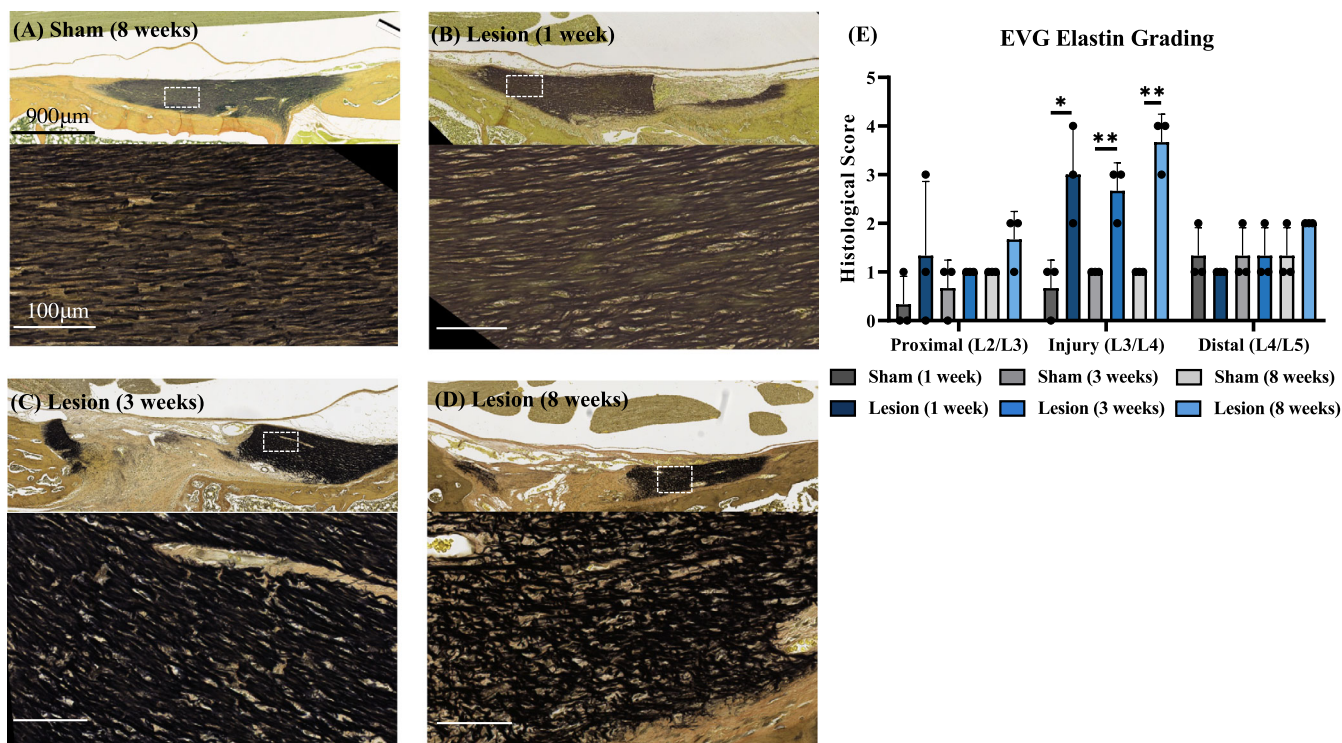


FIGURE 4 Elastin grading of LF hypertrophy following injury. Histological evaluation of elastin using EVG stained histological sections of the LF at midline. Lesion produced a severe loss of elastin (black/brown) alignment and intensity at 1 (B), 3 (C), and 8 weeks (D) when compared to sham (A). At the injury level, lesion produced increases in elastin grading histological scoring across all time points (E). No changes were observed between lesion and sham groups at the adjacent levels. * $p < 0.05$, ** $p < 0.01$, Student's *t*-test. Scale bars as indicated in (A).

Correlation analyses were used to assess potential relationships within varying LF outcome measures and their respective relationship to the IVD. Among the LF histological analyses, medium to large positive correlations were observed between EVG elastin grading and H&E morphological score ($r_s = 0.59$, $p < 0.0001$), EVG elastin grading and MT degree of fibrosis ($r_s = 0.31$, $p = 0.021$), H&E morphological score and LF thickness ($r_s = 0.45$, $p = 0.001$), and H&E morphological score and MT degree of fibrosis ($r_s = 0.32$, $p = 0.017$) (Figure 8). Further, EVG elastin grading had a medium correlation with LF thickness ($r_s = 0.32$, $p = 0.018$) and a small correlation with LF area measurements ($r_s = 0.28$, $p = 0.041$) (Figure 8). Unsurprisingly, LF thickness and area measurements had high correlations ($r_s = 0.86$, $p < 0.0001$) (Figure 8). Lastly, comparing relationships between LF and IVD, there were small to medium negative correlations between disc height changes and EVG elastin grade ($r_s = -0.29$, $p = 0.036$) or H&E morphological score ($r_s = -0.32$, $p = 0.02$, Figure 8).

4 | DISCUSSION

The goal of this study was to investigate the effect of needle scrape injury to rat lumbar LF on longitudinal changes in LF morphology, ECM deposition, fibrosis, and pro-inflammatory expression, simulating LF hypertrophy. The findings of this study show that fluoroscopy-guided needle scrape injury resulted in LF tissue changes over

8 weeks that mimic pathological changes associated with LF hypertrophy. The injury created a disruption of tissue structure, elastin fragmentation and degradation, and promoted immune cell infiltration in the early stages (1 week). Evaluation at later time points also demonstrated a hypertrophic LF tissue that was characterized by increased thickness, disrupted fiber alignment and increased gene expression of pro-fibrotic factors, *Ctgf* and *Tgfb1*. These findings indicate that disruption of the LF created by needle lesion resulted in early pro-inflammatory activation and immune cell infiltration, which resulted in tissue fibrosis that led to LF scar formation. The observed LF fibrosis mimics pathological changes associated with human hypertrophic LF samples. The increased presence of scar tissue is also consistent with findings on ligament injuries throughout the musculoskeletal system, in addition to what has been observed within LF of patients with LSS.^{11-13,33-37} Increases in the fibrosis score of MT-stained human LF sections has been shown to correlate with increases in LF thickness.¹³

Analysis of elastic tissue content within this model revealed a clear loss of elastic tissue staining and elastic fiber fragmentation following injury. A loss of elastic fiber content and alignment, and fiber fragmentation occurs in patient samples with age and with symptomatic LF hypertrophy.^{9,10,14,22,38-40} The regulated control of collagen/elastin composition is vital for proper LF function; The LF fibrosis within this model captured a loss of elastic tissue staining intensity. The evidence for fibrotic matrix in this injury model is further supported by an upregulation of fibrosis related growth factors, *Ctgf* and

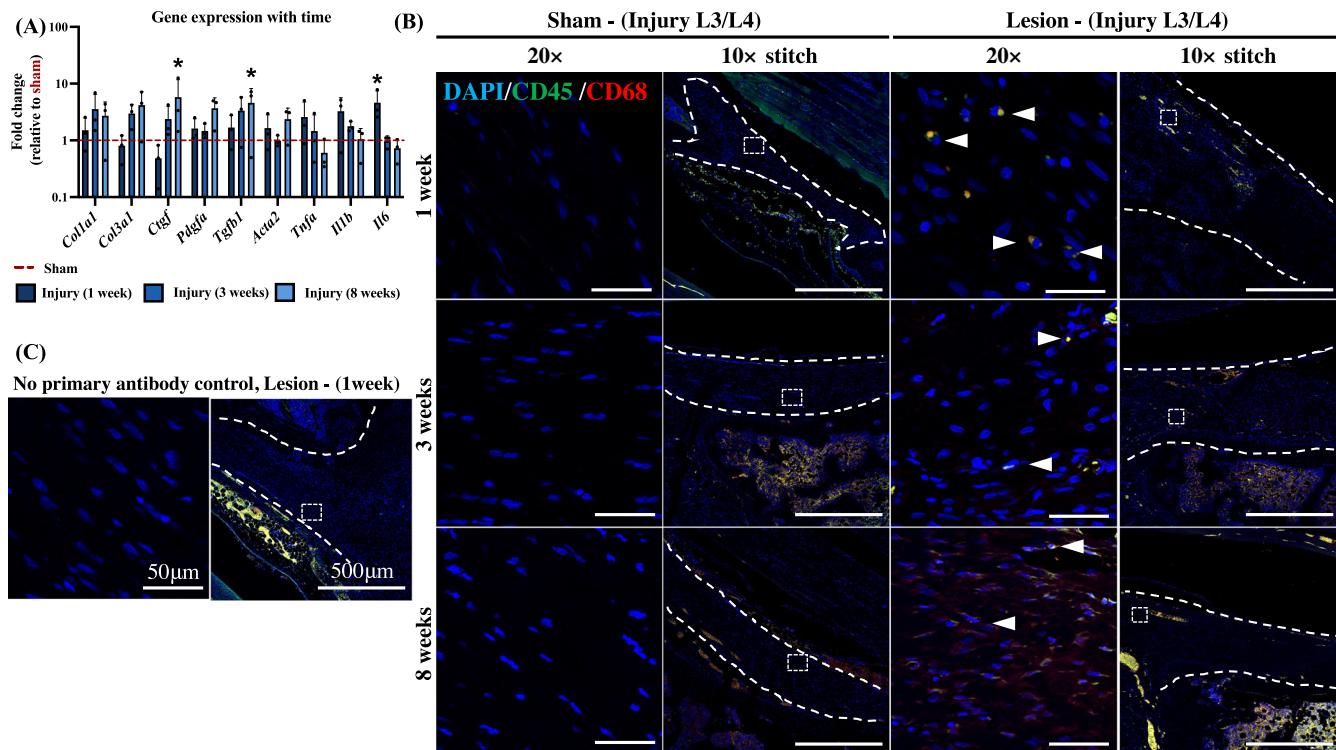


FIGURE 5 Gene expression of hypertrophic and inflammatory markers in lesion LFs relative to sham at the injured level (L3/L4). Lesion produced increased *Il6* (1 week), *Ctgf* (8 weeks) and *Tgfb1* (8 weeks). * $p < 0.05$, Student's *t*-test. (A). Representative IF staining for general leukocyte marker, CD45 (green), and macrophage marker, CD68 (red), in sham and lesion animals (B). Representative no primary control IF images taken at the injury level within the 1 week lesion group (C). Dashed white outline = LF footprint. White arrows indicating positive staining. Scale bars as indicated in (C).

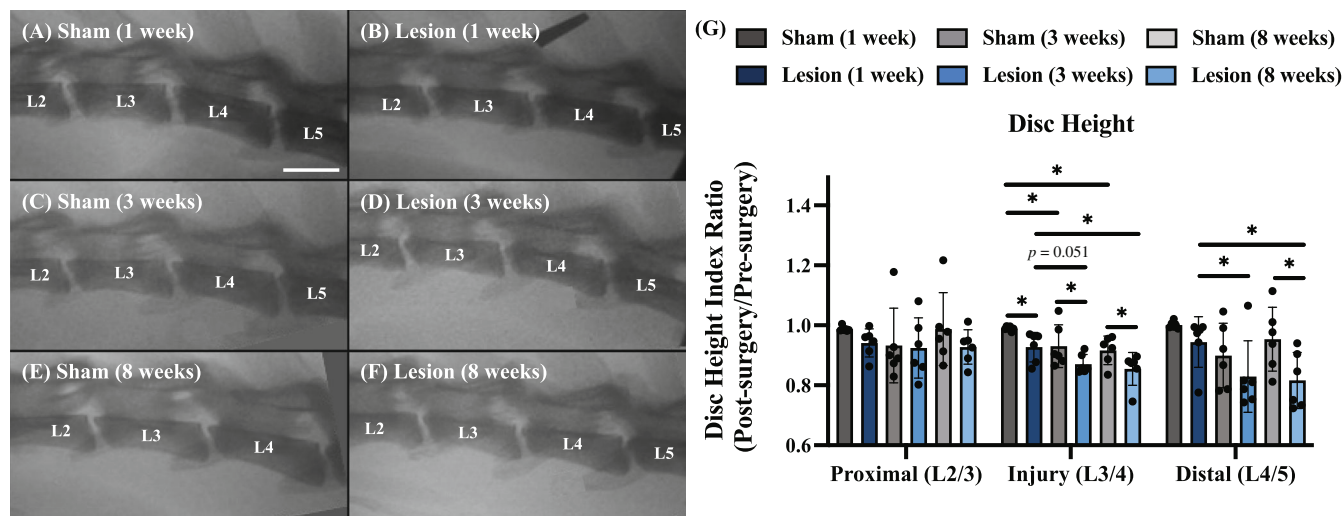


FIGURE 6 Fluoroscopy images of L2-L5 lumbar spine segments taken at post-euthanasia in sham (A, C, E) and lesion (B, D, F) groups. Quantification of DHI ratio revealed significant changes in post-surgery/pre-surgery DHI across surgery groups and time (G). * $p < 0.05$. Student's *t*-test for comparisons across groups within time point. 2-way ANOVA with Fisher's LSD for comparisons within group across time points. Scale bar = 5 mm.

Tgfb1. Previous studies of human hypertrophic LF tissue implicated in LSS have also found upregulation of these hypertrophic markers.²⁰⁻²² The increase of *Tgfb1* expression and histological evidence of LF hypertrophy following injury is consistent with previous animal and

human LF studies, where *Tgfb1* is thought to play a dominant role in promoting collagen production.^{19,25,41} Also captured within this model is an inflammatory response to injury, where CD45⁺/CD68⁺ macrophage cell populations were observed from acute stage (1 week) to

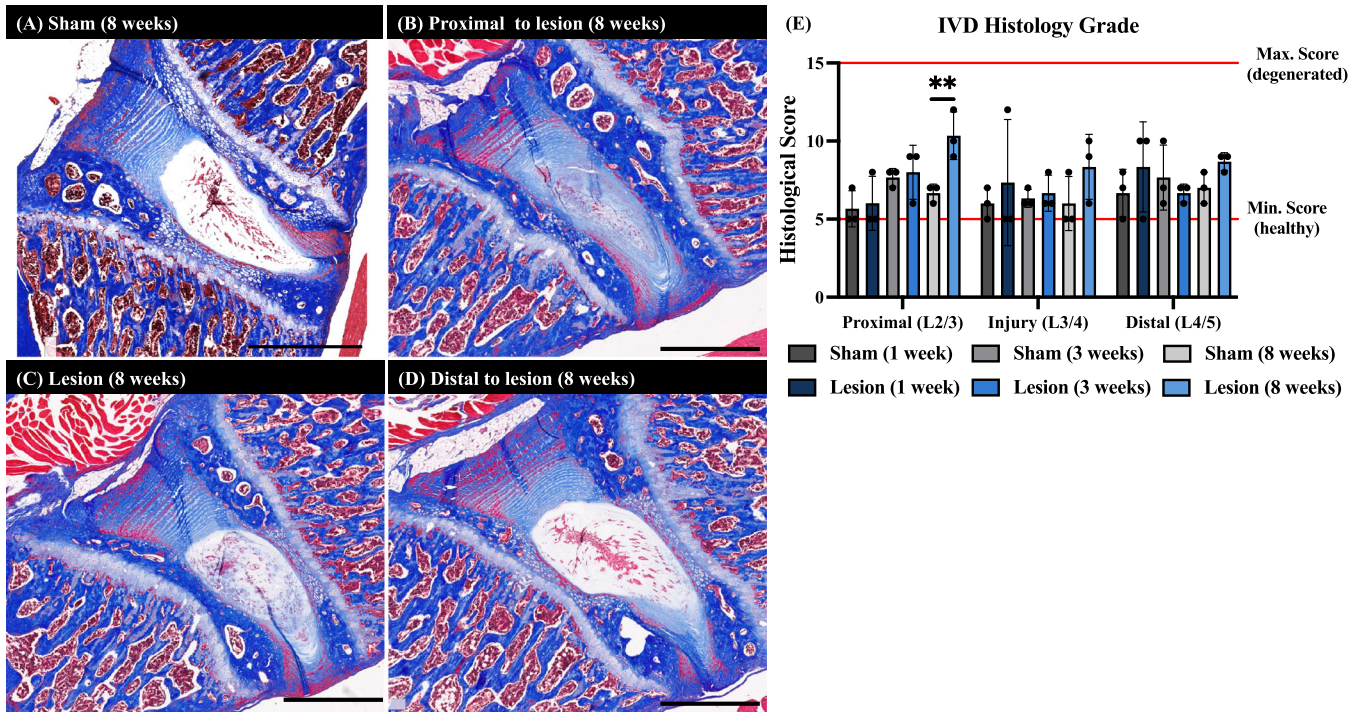


FIGURE 7 Histological scoring of IVD degeneration using MT stained sections of sham and lesion groups at 1, 3, and 8 weeks post-surgery (A–D). Histological analysis revealed a loss of cellularity, cell clustering, and uneven cell distribution within the NP compartment of lesion groups at injury and proximal levels (B). Proximal to lesion at 8 weeks, IVD histological grade was increased in lesion compared to sham (E). * $p < 0.05$. Student's t-test. Scale bar = 1 mm.

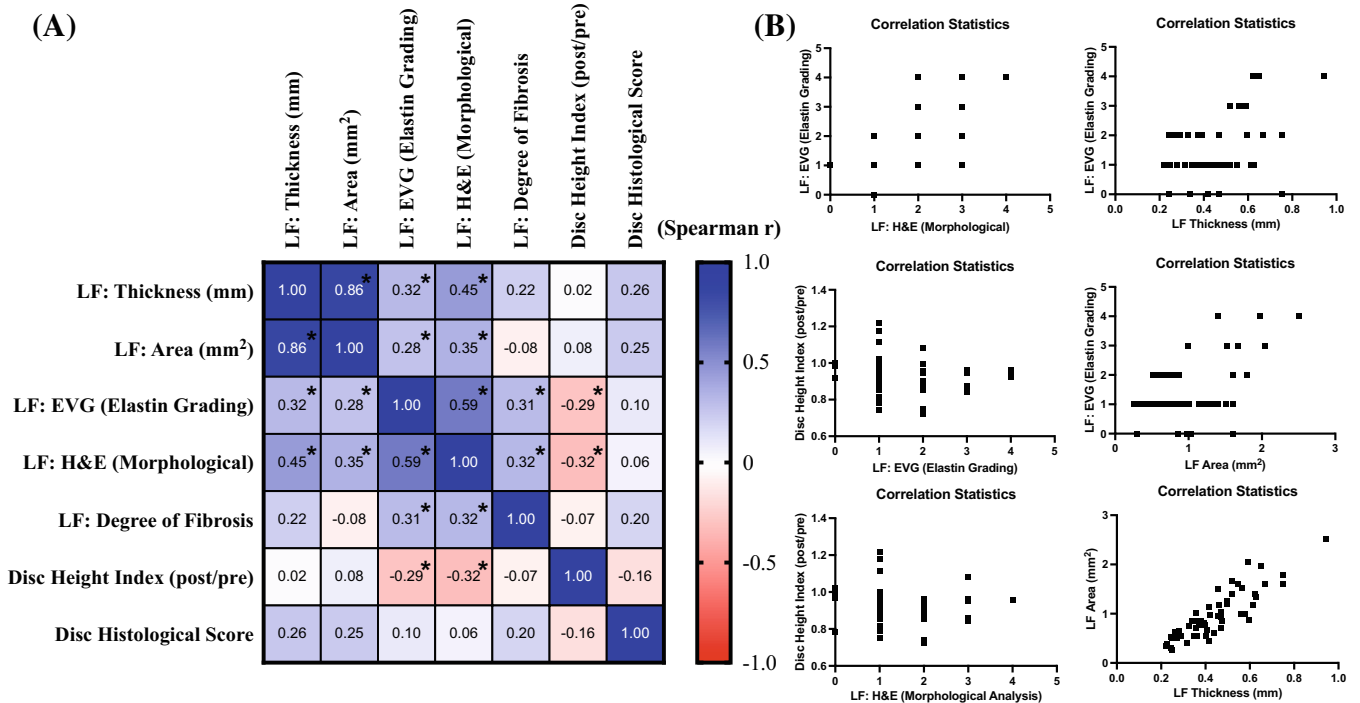


FIGURE 8 Correlation matrix across study outcomes using nonparametric Spearman r_s statistical analysis (A). Outcomes interpreted as small ($0.1 < r_s < 0.29$), medium ($0.3 < r_s < 0.49$) or large ($r_s \geq 0.5$) correlational effect between the measured variables. Significance was observed in correlation data by * $p < 0.05$. Scatter plots indicating significantly ($p < 0.05$) correlated outcomes plotted with a simple linear regression (B).

intermediate (3 weeks) and later sub chronic phases (8 weeks). The innate immune response, specifically interactions with invading macrophages, has been identified as a causative factor in LF hypertrophy via interactions with resident LF cells.²⁶ While the mechanisms driving the fibrotic response characterized by increase in collagen to elastin ratio remain unknown, extensive literature supports the premise that fibroblasts and immune cells, specifically macrophages, reciprocally influence the pathogenesis of fibrosis through cell-cell and secreted factor crosstalk.^{42,43}

Histological analysis throughout the study revealed the presence of an invading cell population, with evidence of CD45⁺/CD68⁺ cells following injury, along with changes in the inflammatory *Il6* gene expression. These changes are likely a contribution of both injured resident cells and the infiltrating immune cells. These findings support the current understanding of the pathogenesis leading to connective tissue hypertrophy, beginning with an innate immune response. Though this model only produced changes in *Il6* gene expression, previous human studies identified an accumulation of inflammatory cells and increases in *IL6* as well as other inflammatory related genes (*COX2*, *IL1B*) following LF hypertrophy.^{13,19} These studies further identified infiltrating macrophages as a primary cell type responsible for elastic tissue degeneration and possibly driven by large increases in *TGFB1* expression.^{13,19} Inflammatory characterization in patient samples is limited to late or end stage disease, however this injury model allows for interactions with a temporal innate immune response which can be investigated for possible immunomodulatory therapies targeting immune cells, like macrophages, which are key players in tissue hypertrophy and chronic inflammation.

In addition to LF hypertrophy, targeted injury of the LF in this model resulted in changes to local IVD integrity. We observed a decrease in IVD height following LF lesion at the injury level across all time points. Degenerative IVD changes were also observed by 8 weeks within the NP compartment at the level proximal to injury. These changes consisted of a loss of cellularity, cell clustering, and uneven distribution of cells within the NP. With ongoing debate about whether LF hypertrophy occurs in isolation or as part of multi-joint spinal changes, the findings of this study suggest that IVD height can be disrupted in response to LF injury, with similar timeline for onset of LF hypertrophy. This is further supported by the findings of the correlation analysis, which found significant moderate correlations between DHI and LF elastin and morphological grade. These findings are consistent with clinical observations where DD was found to be correlated with weakened LF mechanical properties,¹⁶ and increased LF thickness.⁴⁴ Suggesting DD and LF hypertrophic and degenerative changes may be a consequence of disruption to spinal loading mechanisms.

While this study found mild evidence of IVD height loss in sham groups, this was not associated with significant IVD matrix disruption, which ranged in IVD histology grade from 5 to 8 (on a scale ranging from 5 for healthy to 15 for severe degeneration). The sham group IVD histology grade was similar to that found in the uninjured negative control group (IVD histology grade of 7) and exhibits less degenerative structural hallmarks when compared to IVDs from lesion animals.

Though other studies demonstrate that mechanical instability in animal models (e.g., surgical resection of facet joints, supra- and interspinous ligaments) cause IVD degeneration,⁴⁵⁻⁵⁰ the presence of a change in adjacent IVD integrity in the current study was specific to the LF injury groups, compared to sham groups. Therefore, the presence of IVD changes may be due to altered loading at the level of LF injury/hypertrophy. Prior animal models of LF hypertrophy have not explicitly investigated longitudinal multi-joint changes in IVD integrity.²⁵⁻²⁷ To our knowledge, this is the first study to show concomitant onset of LF hypertrophy with multi-level IVD height loss and adjacent IVD degenerative changes after LF needle scrape injury.

Some limitations of this study include that distinct differences exist between rat and human LF tissues, both in size and mechanical functionality. Due to size and mechanical loading differences, the footprint of the LF within the dural tube of rodents is smaller than what is seen in humans, creating limitations in observing severe spinal stenosis. Considering this, although LF tissue thickening was observed in this study, we did not systemically investigate the presence of stenosis of the spinal canal with this LF injury model. Longer time points may be needed for this to occur. Though clear limitations with small animal models exist in recapitulating the human biological and mechanical microenvironment, this model was successful in producing a hypertrophic and fibrotic LF tissue. Another limitation of this study is that the relatively small sample sizes limited our ability to only identify medium to large effects with statistical significance. Future studies will expand the sample size and analyses of this model with additional outcomes beyond the observations made with semi-quantitative grading, gene expression and tissue morphology.

5 | CONCLUSION

In conclusion, this study presents an injury model resulting in the development of a hypertrophic and fibrotic tissue at the site of LF injury in the lumbar rat spine. In doing so this model mimics aspects of the well-characterized human LF hypertrophic condition in both tissue structure and composition. The inflammatory responses observed in this model may be indicative of responses that contribute to the initiation of cellular mechanisms that drive tissue hypertrophy. Lastly, this model captures spinal ligament injury mediated IVD height changes, within adjacent and injury level IVDs, and structural changes within adjacent IVDs.

AUTHOR CONTRIBUTIONS

Kevin G. Burt, Dan C. Viola, and Louis F. Amorosa performed surgeries. Kevin G. Burt, Dan C. Viola, and Lauren E. Lisiewski collected surgical samples and data. Kevin G. Burt, Dan C. Viola, Louis F. Amorosa, Joseph M. Lombardi, and Nadeen O. Chahine analyzed and/or interpreted the data. Kevin G. Burt and Dan C. Viola performed statistical analysis. Kevin G. Burt, Dan C. Viola, and Nadeen O. Chahine drafted and edited the manuscript. All authors have read and approved the final manuscript.

ACKNOWLEDGMENTS

This study was supported in part by the Orthopedic Science and Research Foundation (OSRF), and by funding from the National Institutes of Health (NIH R01AR069668, R01AR077760, R21AR080516). The content is solely the responsibility of the authors and does not necessarily represent the official views of the NIH.

CONFLICT OF INTEREST STATEMENT

The authors declare no conflicts of interest.

ORCID

Kevin G. Burt  <https://orcid.org/0000-0001-8504-7980>

Dan C. Viola  <https://orcid.org/0000-0002-6173-8004>

Lauren E. Lisiewski  <https://orcid.org/0000-0001-9655-7839>

Nadeen O. Chahine  <https://orcid.org/0000-0002-0478-6042>

REFERENCES

- Szpalski M, Gunzburg R. Lumbar spinal stenosis in the elderly: an overview. *Eur Spine J.* 2003;12(2):S170-S175.
- Splettstößer A, Khan MF, Zimmermann B, et al. Correlation of lumbar lateral recess stenosis in magnetic resonance imaging and clinical symptoms. *World J Radiol.* 2017;9(5):223-229.
- Siebert E, Prüss H, Klingebiel R, Failli V, Einhäupl KM, Schwab JM. Lumbar spinal stenosis: syndrome, diagnostics and treatment. *Nat rev Neurol.* 2009;5(7):392-403.
- Lee SY, Kim TH, Oh JK, Lee SJ, Park MS. Lumbar stenosis: a recent update by review of literature. *Asian Spine J.* 2015;9(5):818.
- Towne EB, Reichert FL. Compression of the lumbosacral roots of the spinal cord by thickened ligamenta flava. *Ann Surg.* 1931;94(3):327-336.
- Sakai Y, Ito S, Hida T, Ito K, Harada A, Watanabe K. Clinical outcome of lumbar spinal stenosis based on new classification according to hypertrophied ligamentum flavum. *J Orthop Sci.* 2017;22(1):27-33.
- Munns JJ, Lee JYB, Espinoza Orias AA, et al. Ligamentum flavum hypertrophy in asymptomatic and chronic low back pain subjects. *PLoS One.* 2015;10(5):e0128321.
- Hansson T, Suzuki N, Hebelka H, Gaulitz A. The narrowing of the lumbar spinal canal during loaded MRI: the effects of the disc and ligamentum flavum. *Eur Spine J.* 2009;18(5):679-686.
- Nachemson AL, Evans JH. Some mechanical properties of the third human lumbar interlamellar ligament (ligamentum flavum). *J Biomech.* 1968;1(3):211-220.
- Postacchini F, Gumina S, Cinotti G, Perugia D, DeMartino C. Ligamenta flava in lumbar disc herniation and spinal stenosis. Light and electron microscopic morphology. *Spine.* 1994;19(8):917-922.
- Okuda T, Baba I, Fujimoto Y, et al. The pathology of ligamentum flavum in degenerative lumbar disease. *Spine.* 2004;29(15):1689-1697.
- Sairyo K, Biyani A, Goel V, et al. Pathomechanism of ligamentum flavum hypertrophy: a multidisciplinary investigation based on clinical, biomechanical, histologic, and biologic assessments. *Spine.* 2005;30(23):2649-2656.
- Sairyo K, Biyani A, Goel VK, et al. Lumbar ligamentum flavum hypertrophy is due to accumulation of inflammation-related scar tissue. *Spine.* 2007;32(11):E340-E347.
- Yoshida M, Shima K, Taniguchi Y, Tamaki T, Tanaka T. Hypertrophied ligamentum flavum in lumbar spinal canal stenosis. Pathogenesis and morphologic and immunohistochemical observation. *Spine.* 1992;17(11):1353-1360.
- Chokshi FH, Quencer R, Smoker W. The "thickened" ligamentum flavum: is it buckling or enlargement? *Am J Neuroradiol.* 2010;31(10):1813-1816.
- Cornaz F, Widmer J, Farshad-Amacker NA, Spirig JM, Snedeker JG, Farshad M. Intervertebral disc degeneration relates to biomechanical changes of spinal ligaments. *Spine J.* 2021;21(8):1399-1407.
- Yabe Y, Hagiwara Y, Tsuchiya M, et al. Factors associated with thickening of the ligamentum flavum on magnetic resonance imaging in patients with lumbar Spinal Canal stenosis. *Spine.* 2022;47:1036-1041.
- Safak AA et al. The thickness of the ligamentum flavum in relation to age and gender. *Clin Anat.* 2010;23(1):79-83.
- Löhr M, Hampl JA, Lee JY, Ernestus RI, Deckert M, Stenzel W. Hypertrophy of the lumbar ligamentum flavum is associated with inflammation-related TGF- β expression. *Acta Neurochir.* 2011;153(1):134-141.
- Park J-B, Chang H, Lee J-K. Quantitative analysis of transforming growth factor-beta 1 in ligamentum flavum of lumbar spinal stenosis and disc herniation. *Spine.* 2001;26(21):E492-E495.
- Zhang Y, Chen J, Zhong ZM, Yang D, Zhu Q. Is platelet-derived growth factor-BB expression proportional to fibrosis in the hypertrophied lumbar ligamentum flavum? *Spine.* 2010;35(25):E1479-E1486.
- Zhong ZM, Zha DS, Xiao WD, et al. Hypertrophy of ligamentum flavum in lumbar spine stenosis associated with the increased expression of connective tissue growth factor. *J Orthop Res.* 2011;29(10):1592-1597.
- Hayashi K, Suzuki A, Abdullah Ahmadi S, et al. Mechanical stress induces elastic fibre disruption and cartilage matrix increase in ligamentum flavum. *Sci Rep.* 2017;7(1):1-10.
- Lin C-L, Kuo YT, Tsao CH, Shyong YJ, Shih SH, Tu TY. Development of an in vitro 3D model for investigating ligamentum flavum hypertrophy. *Biol Proced Online.* 2020;22(1):1-12.
- Saito T, Yokota K, Kobayakawa K, et al. Experimental mouse model of lumbar ligamentum flavum hypertrophy. *PLoS One.* 2017;12(1):e0169717.
- Saito T, Hara M, Kumamaru H, et al. Macrophage infiltration is a causative factor for ligamentum flavum hypertrophy through the activation of collagen production in fibroblasts. *Am J Pathol.* 2017;187(12):2831-2840.
- Wang B, Gao C, Zhang P, Sun W, Zhang J, Gao J. The increased motion of lumbar induces ligamentum flavum hypertrophy in a rat model. *BMC Musculoskelet Disord.* 2021;22(1):1-9.
- Sato N, Higashino K, Sakai T, et al. Role of epiligament in ligamentum flavum hypertrophy in patients with lumbar spinal canal stenosis: a pilot study. *J Med Invest.* 2018;65(1.2):85-89.
- Zhang X, Fan X, Zhang Y. Experimental studies on ultramicrostructure of ligamentum flavum at early degeneration. *Orthop J China.* 2006;17(17):1344-1347.
- Han B, Zhu K, Li FC, et al. A simple disc degeneration model induced by percutaneous needle puncture in the rat tail. *Spine.* 2008;33(18):1925-1934.
- Hu W, Kan S, Liu G, Cao Z, Zhu R. The expression of P16 and S100 associated with elastin degradation and fibrosis of the ligamentum flavum hypertrophy. *BMC Musculoskelet Disord.* 2019;20(1):1-8.
- Cohen J. *Statistical Power Analysis for the Behavioral Sciences.* 2nd ed. Lawrence Erlbaum Associate; 1988.
- Majima T, Lo IKY, Randle JA, et al. ACL transection influences mRNA levels for collagen type I and TNF- α in MCL scar. *J Orthop Res.* 2002;20(3):520-525.
- Spindler KP, Murray MM, Detwiler KB, et al. The biomechanical response to doses of TGF- β 2 in the healing rabbit medial collateral ligament. *J Orthop Res.* 2003;21(2):245-249.
- Sakamaki T, Sairyo K, Sakai T, Tamura T, Okada Y, Mikami H. Measurements of ligamentum flavum thickening at lumbar spine using MRI. *Arch Orthop Trauma Surg.* 2009;129(10):1415-1419.
- Capogna G, Celleno D, Simonetti C, Lupoi D. Anatomy of the lumbar epidural region using magnetic resonance imaging: a study of dimensions and a comparison of two postures. *Int J Obstet Anesth.* 1997;6(2):97-100.

37. Botwin KP, Gruber RD. Lumbar spinal stenosis: anatomy and pathogenesis. *Phys Med Rehabil Clin*. 2003;14(1):1-15.
38. Kosaka H, Sairyo K, Biyani A, et al. Pathomechanism of loss of elasticity and hypertrophy of lumbar ligamentum flavum in elderly patients with lumbar spinal canal stenosis. *Spine*. 2007;32(25):2805-2811.
39. Altun I, Yüksel KZ. Histopathological analysis of ligamentum flavum in lumbar spinal stenosis and disc herniation. *Asian Spine J*. 2017;11(1):71-74.
40. Schröder PK et al. Histology of the ligamentum flavum in patients with degenerative lumbar spinal stenosis. *Eur Spine J*. 1999;8(4):323-328.
41. Kalichman L, Cole R, Kim DH, et al. Spinal stenosis prevalence and association with symptoms: the Framingham study. *Spine J*. 2009;9(7):545-550.
42. Mescher AL. Macrophages and fibroblasts during inflammation and tissue repair in models of organ regeneration. *Regeneration*. 2017;4(2):39-53.
43. van Linthout S, Miteva K, Tschöpe C. Crosstalk between fibroblasts and inflammatory cells. *Cardiovasc Res*. 2014;102(2):258-269.
44. Yoshiiwa T, Miyazaki M, Notani N, Ishihara T, Kawano M, Tsumura H. Analysis of the relationship between ligamentum flavum thickening and lumbar segmental instability, disc degeneration, and facet joint osteoarthritis in lumbar spinal stenosis. *Asian Spine J*. 2016;10(6):1132-1140.
45. Oichi T, Taniguchi Y, Soma K, et al. A mouse intervertebral disc degeneration model by surgically induced instability. *Spine*. 2018;43(10):E557-E564.
46. Fukui D, Kawakami M, Yoshida M, Nakao SI, Matsuoka T, Yamada H. Gait abnormality due to spinal instability after lumbar facetectomy in the rat. *Eur Spine J*. 2015;24(9):2085-2094.
47. Lee KE, Thinnis JH, Gokhin DS, Winkelstein BA. A novel rodent neck pain model of facet-mediated behavioral hypersensitivity: implications for persistent pain and whiplash injury. *J Neurosci Methods*. 2004;137(2):151-159.
48. Kaigle AM, Holm SH, Hansson TH. Experimental instability in the lumbar spine. *Spine*. 1995;20(4):421-430.
49. Miyamoto S, Yonenobu K, Ono K. Experimental cervical spondylosis in the mouse. *Spine*. 1991;16(10 Suppl):S495-S500.
50. Stokes I, Counts DF, Frymoyer JW. Experimental instability in the rabbit lumbar spine. *Spine*. 1989;14(1):68-72.

SUPPORTING INFORMATION

Additional supporting information can be found online in the Supporting Information section at the end of this article.

How to cite this article: Burt, K. G., Viola, D. C., Lisiewski, L. E., Lombardi, J. M., Amorosa, L. F., & Chahine, N. O. (2023). An in vivo model of ligamentum flavum hypertrophy from early-stage inflammation to fibrosis. *JOR Spine*, 6(3), e1260. <https://doi.org/10.1002/jsp2.1260>